IAC-22.C1.IPB.21

MULTIPLE-SHOOTING CONTINUATION OF SUN-ASSISTED LUNAR TRANSFERS FROM THE PLANAR BICIRCULAR TO THE EPHEMERIS MODEL

Anastasia Tselousova
Keldysh Institute of Applied Mathematics, RAS, Russian Federation, tselousova@keldysh.ru

Sergey Trofimov
Keldysh Institute of Applied Mathematics, RAS, Russian Federation, trofimov@keldysh.ru
Maksim Shirobokov
Keldysh Institute of Applied Mathematics, RAS, Russian Federation, ovchinni@keldysh.ru

The work is devoted to the problem of adaptation of planar sun-assisted lunar transfer trajectories obtained in the bicircular restricted four-body problem model to the high-fidelity ephemeris model of motion. In addition to the standard gradient multiple-shooting method, which is conventionally used when solving such type of problems, the authors consider the non-gradient modification of the multiple-shooting technique based on the modified Chebyshev-Picard iteration method. The study of the convergence characteristics of both gradient and non-gradient methods is performed on the example of a flight from the low-Earth parking orbit to a lunar near-rectilinear halo orbit.

I. INTRODUCTION

A sun-assisted lunar transfer (SALT), also known as a weak stability boundary transfer or ballistic lunar transfer, is a low-energy transfer to the Moon when a spacecraft departs from a low Earth orbit to a distance far beyond the lunar orbit, undergoes the influence of the solar gravity field, and then heads toward the Moon to be captured ballistically. This type of transfer is characterized by the propellant efficiency and wider launch windows compared to conventional high-energy fast transfers to the Moon. The flight along a SALT trajectory typically takes several months, but requires 200-300 m/s less delta-v. According to Topputo's research, SALT trajectories provide the minimum transfer cost among two-impulse transfers to the Moon in the Earth-Moon-Sun planar bicircular four-body problem (PBR4BP) model, especially when a lunar fly-by included [1].

Such a benefit makes SALT trajectories an attractive option both for the efficient cargo payload delivery to the circumlunar space and for lunar missions of small spacecraft with very limited propellant resources. This type of transfer was used in the Hiten [2] (JAXA, 1990) and GRAIL [3] (NASA, 2011) missions. And just recently, on June 28, 2022, NASA's 12U cubesat CAPSTONE [4] was launched on a four-month SALT trajectory as a pathfinder for the prospective Lunar Gateway space station [5]. Two more cubesats, Japanese EQUULEUS [6] and NASA's Lunar IceCube [7], both using sun-assisted transfers, are scheduled to be launched on September 3, 2022 as a part of Artemis-1 mission [8].

An overview of SALT trajectory design methods can be found in the monograph by J. Parker and R. Anderson [9]. In general case, existing techniques of designing such transfers rely on direct numerical optimization procedures, usually of shooting type. The major challenge is in choosing a good initial guess for that procedures. Previously, we presented several geometrical and analytical tools for the systematic design of SALT trajectories in the PBR4BP model of motion [10, 11]. This model is the simplest one that captures the fundamental geometrical and energy properties of sun-assisted trajectories. Therefore, it can be used for the initial guess trajectory design.

The aim of the current research is to study the problem of adapting SALT trajectories from the PBR4BP to the realistic ephemeris model and specific boundary conditions. The standard tool of trajectory adaptation to a more complex dynamical model is the multiple shooting technique. The resulting system of nonlinear equations is usually solved by some gradient-based method. However, the evaluation of the gradients in the ephemeris model is cumbersome and leads to slow or even poor convergence when using a planar SALT trajectory as an initial guess. So, in addition to the standard multiple shooting procedure, the authors consider the non-gradient modification of the multiple shooting technique based on the modified Chebyshev-Picard iteration method. Up to this mo-

ment, the developed modification of the multiple shooting technique can be used for solving boundary value problems without optimization. However, it gives a smooth solution from the vicinity of the Earth to the vicinity of the Moon, which is then can be fed as an initial guess to the gradient method to obtain an exact solution.

In this work, the above-described approaches are compared for the flight from the Baikonur launch parking orbit (h = 200 km, i = 51.6 deg) to the L_2 southern near-rectilinear halo orbit (NRHO) 9:2, the primary candidate for the nominal orbit in the ongoing Lunar Gateway project.

II. SALT GENERATION IN PBR4BP MODEL

II.I Planar bicircular restricted four-body problem

The planar bicircular restricted four-body problem models the motion of the spacecraft of negligible mass under the gravitational pull of three massive bodies, the Earth, the Moon, and the Sun in our case. In this model, the Earth (with the mass m_E) and the Moon (m_M) are revolving with a constant angular velocity in circular coplanar orbits around their center of mass C. The Sun (m_S) is assumed to revolve in a circular orbit of radius $L \gg 1$ around C in the same plane (see Fig. 1). The motion of the spacecraft also occurs in this plane. In the standard Earth-Moon rotating reference frame with the x-axis connecting m_E and m_M, the equations of motion are written as

$$\ddot{x} - 2\dot{y} = \frac{\partial \Omega_4}{\partial x}, \quad \ddot{y} + 2\dot{x} = \frac{\partial \Omega_4}{\partial y} \qquad [1]$$

where

$$\Omega_4 = \Omega_3 + \frac{\mu_S}{r_3} - \frac{\mu_S}{L^2}(x\cos\theta + y\sin\theta) \qquad [2]$$

is the effective potential. The equations [1] are written in the dimensionless system of units in which 1) masses are normalized so that $m_E = 1 - \mu$ and $m_M = \mu$ where $\mu = m_M/(m_E + m_M)$, 2) the angular velocity of the rotating frame is normalized to one, and 3) the distance between m_E and m_M is normalized to one. Thus, the dimensionless universal gravitational constant G is also identically equal to one. In this system of units, m_E and m_M are at fixed positions along the x-axis at $[-\mu, 0]$ and $[1-\mu, 0]$, respectively. For the Earth-Moon system, the units of distance, velocity and time are the following:

$$\text{DU} = 384402 \text{ km},$$
$$\text{VU} = 1.024544182251307 \text{ km/s},$$
$$\text{TU} = 4.342513772754916 \text{ days}.$$

The mass parameter

$$\mu = 0.012150584460351,$$

the gravitational parameter of the Sun

$$\mu_S = 3.289005596145305 \times 10^5.$$

The spacecraft distances to m_E, m_M and m_S are given by the equalities $r_1^2 = (x+\mu)^2 + y^2$, $r_2^2 = (x-1+\mu)^2 + y^2$, $r_3^2 = (x - L\cos\theta)^2 + (y - L\sin\theta)^2$, respectively. The phase of the Sun θ defines the position of the Sun in the Earth-Moon system; this angle linearly grows over time: $\theta = \theta_0 + \omega_S(t - t_0)$. For L = 389.17 (the approximate Earth-Sun distance), the orbital velocity of the Sun is determined as $\omega_S = \sqrt{(1+m_S)/L^3} - 1 \approx \approx -0.9253$.

When the last two terms in the effective potential [2] are discarded, the BR4BP model is reduced to the well-known planar circular restricted three-body problem (CR3BP) model with the effective potential $\Omega_3 = (x^2+y^2)/2 + (1-\mu)/r_1 + \mu/r_2 + \mu(1-\mu)/2$.

II.II Designing SALT transfers in PBR4BP model

Let us briefly describe the methodology based on which SALT trajectories are calculated in the framework of the PBR4BP model. At the first stage, a sun-assisted trajectory is divided into three parts using the concept of *regions of prevalence*. According to Castelli [12], the boundary of the Earth-Moon region of prevalence consists of points in the configuration space where the error in the right-hand side of the spacecraft's equations of motion would have the same magnitude independently of what body we neglect in the Earth-Moon-Sun system—the Moon or the Sun. In a planar case, the boundary of the region of prevalence can be mean-square approximated by an ellipse in the Earth-Moon rotating reference frame [11]. Figure 2 shows the Earth-Moon region of prevalence boundaries for different Sun phase angles and the orange elliptical boundary of the mean-square averaged region of prevalence. So, a SALT trajectory is divided into the three legs: the arriving and departing legs, lying inside the region of prevalence and calculated in the Earth-Moon PCR3BP model, and the exterior leg, designed in the Earth-Moon-Sun PBR4BP model.

The use of the PCR3BP within the region of prevalence allows one to take advantage of important dynamical properties of this model. In particular, the PCR3BP system has an integral of motion, the Jacobi integral,

$$J_{EM} = 2\Omega_3 - (\dot{x}^2 + \dot{y}^2),$$

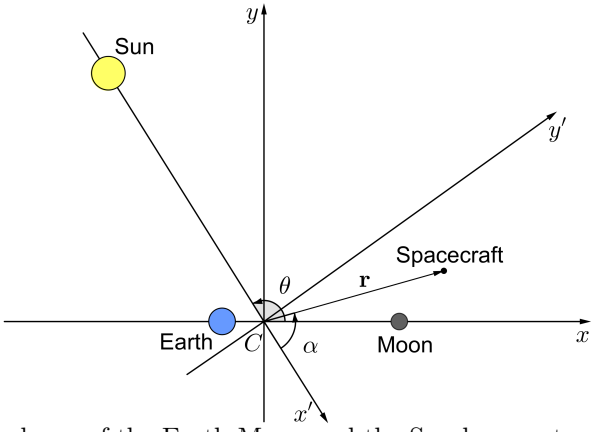

Fig. 1: The Cxy and $Cx'y'$ planes of the Earth-Moon and the Sun-barycenter rotating reference frames.

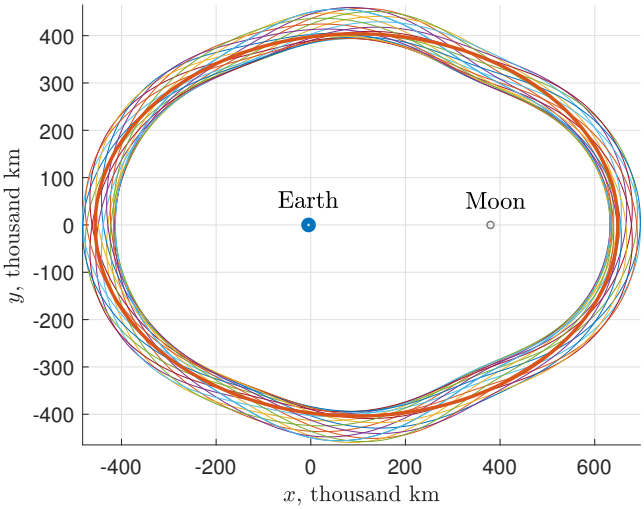

Fig. 2: Earth-Moon region of prevalence boundaries for different Sun phase angles and the orange elliptical boundary of the mean-square averaged region of prevalence.

and, thus, any solution lies on the manifold $\mathcal{J}(\widetilde{J}_{EM}) = \{[x, y, \dot{x}, \dot{y}] \in \mathbb{R}^4 \mid J_{EM}(x, y, \dot{x}, \dot{y}) = \widetilde{J}_{EM}\}$ for some energy level $\widetilde{J}_{EM}$.

As it is well known, for a planar trajectory to be transit (i.e., passing inside the lunar Hill sphere), it should belong to the interior of the stable manifold tube of the planar Lyapunov orbit with the corresponding Jacobi integral level [9]. In the $(x, \dot{x})$ plane, the manifold trajectories, when crossing the Earth-Moon region of prevalence boundary, form a closed curve limiting the L_2 lunar gateway (Fig. 3). Let P denote a set of inner points of the gateway. Note that for any point of P and a given $[x_P, \dot{x}_P]$, the corresponding coordinate y_P can be found from the condition of belonging to the region of prevalence boundary, while $\dot{y}_P$ is determined by the energy relation $J_{EM}(x_P, y_P, \dot{x}_P, \dot{y}_P) = \widetilde{J}_{EM}$. The propagation of the initial condition $\mathbf{x}_P = [x_P, y_P, \dot{x}_P, \dot{y}_P]$ in the CR3BP model will give a trajectory passing inside the Hill sphere of the Moon.

Each point $\mathbf{x}_P$ produces a trajectory with a certain value of the perilune distance r_p and the argument of the perilune ω_p (in the planar case, the angle between the Cx axis of the Earth-Moon rotating reference frame and the direction Moon-perilune). It is convenient to display initial data for the trajectories with a given value of r_p and/or ω_p on the lunar gateway in the form of gradient-colored contour lines. Figure 3 shows the line $r_p = 3141$ km on the L_2 gateway with $J_{EM} = 3.06$. Such values of the Jacobi integral and perilune distance coincide with the values for the NRHO 9:2. The color of the contour line points indicates the ω_p value of the approaching trajectory. Consequently, to obtain the arriving leg with specified r_p and ω_p values,

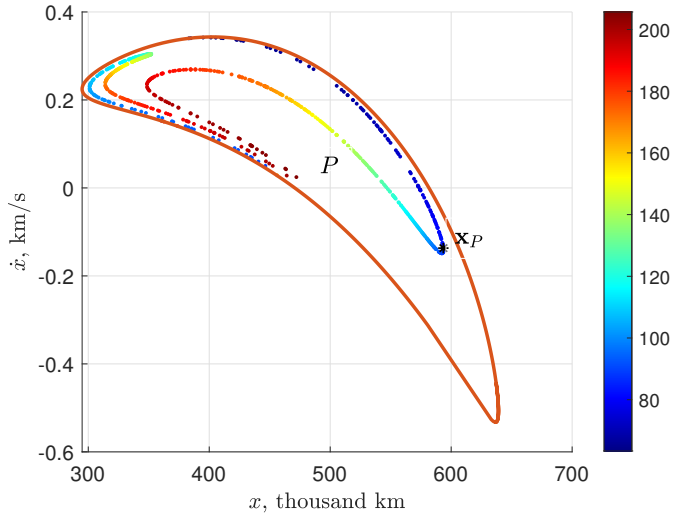

Fig. 3: L_2 lunar gateway for $J_{EM} = 3.06$ (orange closed curve).

the corresponding point of P should be targeted. At the preliminary stages of designing a transfer to the NRHO orbit, it is possible to target all points of a given isoline to form initial guess trajectories.

For a given point $\mathbf{x}_P$, the phase of the Sun θ_P specifies a certain exterior leg outside the region of prevalence when propagating $\mathbf{x}_P$ in the PBR4BP model backward in time. If, for some value of θ_P, the corresponding exterior leg intersect the boundary of the region of prevalence at some point $\mathbf{x}_P^B = \mathbf{x}_P^B(\mathbf{x}_P, \theta_P)$, we try to retrieve a departing leg which provides a zero residue with $\mathbf{x}_P^B$ by varying the departure trajectory parameters. Here we consider a circular 200 km orbit as a departing, so the trans-lunar injection (TLI) impulse Δv_{TLI} and the point of its application (defined by the angle φ) fully determine a spacecraft trajectory inside the region of prevalence. Let us denote the point obtained by integrating the departing leg until the intersection with the region of prevalence as $\mathbf{x}_D^B = \mathbf{x}_D^B(\Delta v_{TLI}, \varphi)$. On the boundary of the region of prevalence, the point $\mathbf{x}_P^B$ is patched with the point $\mathbf{x}_D^B$ so that $|\mathbf{x}_P^B - \mathbf{x}_D^B| < 10^{-4}$. As a result, we obtain an initial guess SALT trajectory.

Subsequently, it is adapted to the BR4BP model by the multiple shooting method: the trajectory is divided into $N+1$ nodes, $0 = t_0 \leq \ldots \leq t_N = t_f$, where t_f is the time of flight, so the non-linear programming problem arises. We require that $\Delta v_{TLI} \leq 3.2$ km/s and $\Delta v_{TCM} \to \min$, where Δv_{TCM} is an additional trajectory correction maneuver (TCM) at the trajectory apoapsis. The final lunar orbit insertion (LOI) impulse Δv_{LOI} is set to zero. The equality-type constraints include conditions for smoothness of patching the position and velocity at internal nodes of the multiple shooting method, at the initial epoch t_0 the phase vector belongs to a given near-Earth parking orbit, and the final state should be at the periapsis of a given lunar orbit. A detailed description of solving the corresponding non-linear programming problem can be found in the authors' previous work [11].

II.III Planar SALT trajectories

Using the presented methodology, a database of SALTs to different orbits around the Moon was obtained in the PBR4BP model. For all SALT trajectories, its apogees are located in the second or fourth quadrant of the Sun-barycenter rotating reference frame $Cx'y'$ where $\sin 2\alpha < 0$ (see Fig. 1). Under this condition, the gravitational perturbation from the Sun provides $\Delta J_{EM} > 0$ along the exterior leg, which is a necessary condition for subsequent ballistic capture. This well-known result of the SALT theory, previously numerically discovered by many researchers, has been also analytically explained in the framework of the PBR4BP model [10].

The database contains, among others, transfers with lunar flybys. Generally, SALTs can be divided into three groups: without intermediate lunar flybys (I), and with an outbound leading (II) or trailing (III) side flyby (see Fig. 4). For the trajectories from a circular 200 km near-Earth parking orbit to the lunar orbits with $J_{EM} = 3.06$ and $r_p = 3141$ km, the characteristic time of flight turned out to be from 70 to 250 days for lunar-gravity-assisted transfers and from 85 to 210 days for SALTs with-

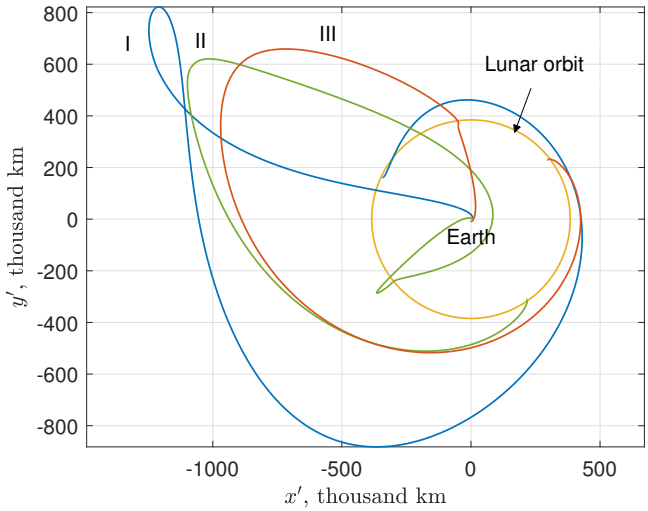

Fig. 4: Examples of typical planar SALT trajectories.

out flybys. It is worth noting that a lunar gravity assist significantly reduces the launch energy C_3: from $-0.74...0.62$ km^2/s^2 for a simple SALT to $-2.03...1.03$ km^2/s^2 for trajectories with lunar flybys.

Figure 4 shows typical examples of planar trajectories of each type. The blue line corresponds to the sun-assisted transfer without flyby with time of flight equal to 167 days, $\Delta v_{TLI} = 3.19$ km/s and $\Delta v_{TCM} = 11.56$ m/s. Green line represents lunar-gravity-assisted transfer with leading side flyby (105 days, $\Delta v_{TLI} = 3.15$ km/s, $\Delta v_{TCM} = 26.31$ m/s). The third type of SALT is depicted in orange (82 days, $\Delta v_{TLI} = 3.17$ km/s, $\Delta v_{TCM} = 16.77$ m/s). Symmetrical trajectories can be designed with the apogee in the fourth quadrant.

III. MULTIPLE SHOOTING ADAPTATION TO THE EPHEMERIS MODEL

III.I High-fidelity model of orbital motion

The high-fidelity ephemeris model of motion is used to provide high accuracy modeling. It includes the central gravitational fields of the Earth and the Moon, gravitational perturbations from the Sun and all the planets of the Solar system, as well as solar radiation pressure.

In the Geocentric Celestial Reference System (GCRS) gravitational accelerations from a certain celestial body can be written as

$$\mathbf{a}_B = \frac{\mu_B}{|\mathbf{r}_B - \mathbf{r}|^3}(\mathbf{r}_B - \mathbf{r}) - \frac{\mu_B}{|\mathbf{r}_B|^3}\mathbf{r}_B \qquad [3]$$

where μ_B is the gravitational parameter of the considered celestial body and $\mathbf{r}_B$ is its radius vector. For the Earth, the second term in [3] is equal to zero because of $\mathbf{r}_B = 0$. The solar radiation pressure (SRP) acceleration is determined as

$$\mathbf{a}_{SRP} = -\frac{\delta P A}{m}\frac{\mathbf{r}_S - \mathbf{r}}{|\mathbf{r}_S - \mathbf{r}|^3}\varkappa^2.$$

Here $\delta \in [0;1]$ represents the level of illumination, and the constant $P = 4.56 \cdot 10^{-6}$ Pa can be interpreted as solar radiation pressure at $\varkappa = 1$ a.u. distance from the Sun. The area-to-mass ratio $A/m = 0.006$ m^2/kg is taken.

So, the spacecraft's equations of motion in the GCRS are the following:

$$\ddot{\mathbf{r}} = \sum_B \mathbf{a}_B + \mathbf{a}_{SRP}. \qquad [4]$$

The gravitational parameters of the Solar system's celestial bodies can be found in the Astronomical Almanac 2018.* In this work, their positions and velocities are determined from JPL's DE430 ephemeris [13].

III.II Standard adaptation procedure

Now let us focus on the problem of adaptation of planar SALT trajectories to the realistic three-dimensional model. Using the multiple-shooting method, the three-dimensional trajectory design is reduced to solving a non-linear programming problem. The epochs and state vectors of the spacecraft in the GCRS coordinate system, as well as the LOI impulse and TCM, are selected as the optimization

*http://asa.usno.navy.mil/

variables. The initial guess for the phase variables consists of the epochs and state vectors of the spacecraft retrieved from the planar solution, the initial guess for impulses can also be set as in the planar case. As the objective function, the sum of the squares of the TCM and LOI impulses is considered: $\Delta v_{TCM}^2 + \Delta v_{LOI}^2 \to \min$. The constraints of the multiple shooting method include requirements for

- the altitude, inclination, and eccentricity of a post-launch parking near-Earth orbit,
- the launch date and time,
- the departure impulse magnitude,
- smoothness of patching the position and velocity at all internal nodes of the multiple shooting method,
- conditions for entering the target orbit.

A circular 200 km orbit is taken as a low-Earth parking orbit where a transfer to the Moon begins by applying the TLI maneuver. The parking orbit corresponds to the launch from the Baikonur cosmodrome and is fixed relative to the International Terrestrial Reference System axes: its inclination is 51.6°, the longitude of the ascending node is 8.26 E. The magnitude of the TLI impulse has an upper limit of 3.2 km/s. What concerns the final lunar orbit, the L_2 southern NRHO 9:2 is assumed. We require that the final position and velocity of the spacecraft correspond to the average perilune of the NRHO orbit in the rotating Earth-Moon reference frame. The launch date is selected in accordance with the resulting value of the phase of the Sun θ_0 at the initial epoch for the corresponding planar initial-guess trajectory. In general, for a particular transfer, θ_0 corresponds to 12 launch dates within a year. Further, for certainty, the launch dates in August 2028 are considered.

III.III Modified adaptation procedure using the Chebyshev-Picard method

Among well-established non-gradient methods that allow solving boundary value problems, it is worth noting the modified Chebyshev–Picard iteration method. It is based on the principle of contraction mappings. The main idea of this method is to approximate the right-hand sides of the equations of motion by a sum of Chebyshev polynomials and then integrate the system of equations in Picard iterations [14].

The Chebyshev-Picard method has found its application in solving astrodynamical problems [15]. However, its main disadvantage is known to be the limited area of convergence. The use of the multiple shooting technique makes it possible to expand the region of convergence and thus, obtain a non-gradient method for solving boundary value problems on any given time interval. This subsection describes a non-gradient version of the multiple shooting method based on the Chebyshev–Picard iterations. The multiple shooting method is considered in relation to the system of ordinary non-linear differential equations [4] for solving a boundary value problem $\mathbf{r}(t_0) = \mathbf{r}_0, \quad \mathbf{r}(t_f) = \mathbf{r}_f$.

First, we divide the time interval $[t_0; t_f]$ into N subintervals $[t_i; t_{i+1}]$, $i = 0,\ ...,\ N-1$, so that the modified Chebyshev–Picard iteration method converges for the following boundary value problems:

$$\mathbf{r}(t_i) = \mathbf{r}_i, \quad \mathbf{r}(t_{i+1}) = \mathbf{r}_{i+1} \quad (I);$$
$$\mathbf{r}(t_i) = \mathbf{r}_i, \quad \mathbf{v}(t_{i+1}) = \mathbf{v}_{i+1} \quad (II);$$
$$\mathbf{v}(t_i) = \mathbf{v}_i, \quad \mathbf{r}(t_{i+1}) = \mathbf{r}_{i+1} \quad (III).$$

A detailed description of the Chebyshev-Picard method for solving these boundary value problems is given in Appendix A.

To patch the trajectory at the nodes of the multiple shooting method, the following rules for updating velocities and positions are introduced. Let $\mathbf{v}_i^{i+1}(t_i)$ be the departure velocity from the point t_i to the point t_{i+1}, $i = 0,\ ...,\ N-1$, and $\mathbf{v}_i^{i-1}(t_i)$ be the arrival velocity to the point t_i from the point t_{i-1}, $i = 1,\ ...,\ N$. A similar notation for the radius vector is also introduced. As a result of solving the problem of type I on each subinterval, we obtain $\mathbf{v}_i^{i+1}(t_i)$ and $\mathbf{v}_{i+1}^{i}(t_{i+1})$. The velocity residual at the interior node t_i is defined then as $||\mathbf{v}_i^{i+1}(t_i) - \mathbf{v}_i^{i-1}(t_i)||$, $i = 1,\ ...,\ N-1$, where $||.||$ is the Euclidean norm. The condition for patching the solution in terms of velocity with accuracy ε can be written as

$$\max_{i=1,\ \dots\ ,N-1} \left\|\mathbf{v}_i^{i+1} - \mathbf{v}_i^{i-1}\right\| < \varepsilon.$$

The updated velocity is defined as

$$\mathbf{v}_i^{new} = \frac{\mathbf{v}_i^{i+1} + \mathbf{v}_i^{i-1}}{2},\ i = 1,\ ...,\ N-1, \qquad \mathbf{v}_0^{new} = \mathbf{v}_0^1,\ \mathbf{v}_N^{new} = \mathbf{v}_N^{N-1}. \qquad [5]$$

Using the updated velocity values, it is also possible to solve problems of type II and III on each subinterval. The solution of these problems provides $\mathbf{r}_{i+1}^{i}(t_{i+1})$ and $\mathbf{r}_i^{i+1}(t_i)$, $i = 0,\ ...,\ N-1$, respectively. By analogy, the condition for patching

the solution in terms of radius vector with accuracy ε can be written as

$$\max_{i=1,\ \dots\ ,N-1} \left\| \mathbf{r}_i^{i+1} - \mathbf{r}_i^{i-1} \right\| < \varepsilon.$$

The updated radius-vector is defined as

$$\mathbf{r}_i^{new} = \frac{\mathbf{r}_i^{i+1} + \mathbf{r}_i^{i-1}}{2}, \qquad [6]$$
$$\mathbf{r}_0^{new} = \mathbf{r}_0,\ \mathbf{r}_N^{new} = \mathbf{r}_N.$$

Using the rules [5] and [6], the full algorithm can be written as follows. Let R, V be arrays of vectors of size $3 \times (N+1)$ whose columns define positions and velocities at time nodes, ΔR, ΔV — arrays of size $1 \times (N+1)$ whose components define position and velocity residuals. We also introduce the learning rate, $lr \in [0;1]$, which specifies the principle for modifying an array of radius vectors as $R \leftarrow R + (R_{new} - R)\, lr$, R_{new} is obtained after applying the update rules. Further, the designation *updating* corresponds to the rule according to which the array of velocities V_{new} is updated by the array of positions R; the array of positions R_{new} is updated by the array of positions R and the array of velocities V. The corresponding errors are defined as ΔV_{new}, ΔR_{new}.

The *correction* and *average* procedures allow one to improve the described rules for updating positions and velocities. In the first one, positions or velocities are updated only at those nodes where the new residual is reduced compared to the previous iteration. The *average* procedure updates the arrays of positions and velocities by calculating the average value over the last few iterations.

We also introduce verification and patching conditions:
matching — condition for patching the solution with the required accuracy ε

$$||\Delta R|| = \max_{i=1,\ \dots\ N-1} \Delta R_i < \varepsilon,$$
$$||\Delta V|| = \max_{i=1,\ \dots\ N-1} \Delta V_i < \varepsilon,$$

check — check for residual reduction at each iteration

$$||\Delta R_{new}|| < ||\Delta R||, \quad ||\Delta V_{new}|| < ||\Delta V||.$$

The pseudocode of the method is given in Appendix B.

This version of the multiple shooting technique does not include velocity optimization, however, it provides a smooth quasi-planar solution from the vicinity of the Earth to the vicinity of the Moon, which can then be refined by the gradient method described in the subsection III.II.

IV. RESULTS

Both of the above approaches have been applied to adapt planar SALT trajectories to the realistic ephemeris model of motion. All the algorithms are implemented in MATLAB. The arising non-linear programming problems are solved using the *sqp* option of MATLAB's `fmincon` solver.

It should be noted that the convergence of multiple shooting procedures strongly depends on the choice of optimization nodes. The authors used an empirical rule for choosing the nodes based on the analysis of the convergence of multiple-shooting method for trajectories with various times of flight. The initial base of trajectories from the first stage of planar SALT trajectory design was obtained using the MATLAB's `ode113` integrator with the absolute and relative integration tolerances of 10^{-12}. Moreover, trajectories from this base had an adaptive time step based on the integration tolerance on the departing and arriving legs, and the fixed step of 14 hours on the exterior leg. For these parameters, every one out of 10 points was taken as an optimization node on the departing leg, every one out of 2000 points — on the exterior leg, and every one out of 15 points — on the arriving leg. Thus, the number of nodes for the initial-guess trajectories varied from 50 to 90, depending on the time of flight. Such discretization provides high convergence both for adaptation to the bicircular model of motion and for the subsequent adaptation to the ephemeris model of motion.

Let us present the results of multiple-shooting adaptation of planar SALT trajectories without lunar gravity assist to the ephemeris model of motion. For the base of 150 trajectories with different times of flight, as a result of applying the simple multiple-shooting technique, 47 realistic three-dimensional SALT trajectories from the Baikonur parking orbit to the southern NRHO 9:2 with $\Delta v_{TCM} + \Delta v_{LOI} < < 100$ m/s have been obtained (31% of the total number of trajectories). The use of the multiple-shooting procedure based on the modified Chebyshev-Picard iteration method has increased the percentage of convergence up to 56%. The modified Chebyshev-Picard iteration method was used with the following parameters: for all the interior subintervals $P = 5$, $M = 5$, $\varepsilon = 10^{-3}$ (see Appendix A), and when patching a trajectory, $lr = 0.01$, $\varepsilon = 10^{-3}$. These parameters and the above described procedure for selecting the optimization nodes ensured the convergence of the modified Chebyshev-Picard iteration method in 90% of cases.

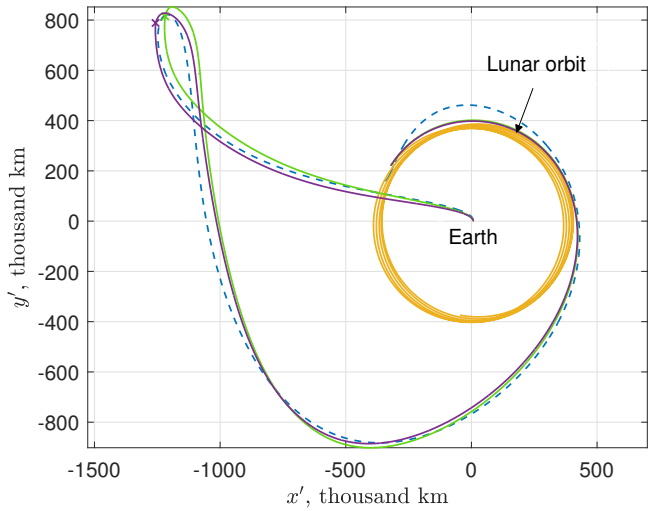

Fig. 5: An example of initial-guess planar SALT trajectory (blue dashed line) and the resulting realistic transfer trajectories obtained by the simple multiple-shooting technique (purple line) and using the modified Chebyshev-Picard iteration method (green line).

For a computer system with Intel(R) Core(TM) i5-8265U CPU, 1.8 GHz, 16 GB RAM, the convergence time of the simple multiple-shooting method varied from 10 to 40 minutes. In this case, the integration of the equations of motion was carried out using 4 computer cores. Leveraging the modified Chebyshev-Picard iteration method slows down the adaptation process: its convergence takes up to 30 minutes. After that, the trajectory is refined by the gradient method, which also requires from 10 to 40 minutes. To speed up the running time, the modified Chebyshev-Picard iteration method can be parallelized, however, this is a matter for future research.

The solutions obtained by the two multiple-shooting techniques are slightly different. In most of cases, when using the modified Chebyshev–Picard iteration method, a trajectory with less delta-v is obtained. Figure 5 shows an example of initial-guess planar SALT trajectory (blue dashed line) and the resulting realistic transfer trajectories obtained by the simple multiple-shooting technique (purple line) and using the modified Chebyshev–Picard iteration method (green line). For both transfers the launch date is August 26, 2028, 12:23:09, and the arrival date is 10 February, 2029, 10:31:13. For the purple trajectory $\Delta v_{TLI} = 3.2$ km/s, $\Delta v_{TCM} = 27.9$ m/s, $\Delta v_{LOI} = 71.6$ m/s. The cross indicates the point of executing of the trajectory correction maneuver. The green trajectory is characterized by $\Delta v_{TLI} = 3.2$ km/s, $\Delta v_{TCM} = 23.3$ m/s, $\Delta v_{LOI} = 33.1$ m/s.

V. CONCLUSION

This work is focused on the issue of adaptation of planar SALT trajectories obtained in the PBR4BP model to the high-fidelity ephemeris model of motion. The authors considered two adaptation strategies: the standard gradient multiple-shooting method and the developed non-gradient modification of the multiple-shooting technique with the subsequent gradient adjustment. In the second case, the modified Chebyshev–Picard iteration method is used to solve the resulting boundary value problems. The study of the convergence characteristics was carried out for 150 trajectories of different time of flight without a lunar gravity assist from the Baikonur parking orbit to the southern NRHO 9:2.

The use of the modified Chebyshev-Picard iteration method made it possible to increase the percentage of convergence by 25%. However, the runtime may be increased up to 40 minutes. In the future, this time can be reduced by parallelizing the method.

VI. Acknowledgments

This work is fully supported by the Russian Science Foundation grant 19-11-00256.

Appendix A

Here we describe the Chebyshev-Picard method for solving the system of ordinary non-linear equations of the second order

$$\ddot{\mathbf{r}} = \mathbf{f}(t, \dot{\mathbf{r}}(t), \mathbf{r}(t)), \quad t \in [t_0, t_f],$$

with one of the following boundary value problems:

$$\begin{array}{ll} \mathbf{r}(t_0) = \mathbf{r}_0, & \mathbf{r}(t_f) = \mathbf{r}_f \\ \mathbf{r}(t_0) = \mathbf{r}_0, & \dot{\mathbf{r}}(t_f) = \mathbf{v}_f \\ \dot{\mathbf{r}}(t_0) = \mathbf{v}_0, & \mathbf{x}(t_f) = \mathbf{r}_f. \end{array}$$

First, the transition to a new independent variable τ is done:

$$t = \omega_1 + \omega_2 \tau, \quad \omega_1 = \frac{t_0 + t_f}{2}, \quad \omega_2 = \frac{t_f - t_0}{2}.$$

Thus, the boundary value problem is rewritten as

$$\ddot{\mathbf{r}} = \mathbf{g}(\tau, \dot{\mathbf{r}}(\tau), \mathbf{r}(t)) \equiv \omega_2^2 \mathbf{f}(t, \dot{\mathbf{r}}(t), \mathbf{r}(t)), \quad \tau \in [-1, 1], \qquad [7]$$

$$\begin{array}{ll} \mathbf{r}(-1) = \mathbf{r}_0, & \mathbf{r}(1) = \mathbf{r}_f \\ \mathbf{r}(-1) = \mathbf{r}_0, & \dot{\mathbf{r}}(1) = \mathbf{v}_f \\ \dot{\mathbf{r}}(-1) = \mathbf{v}_0, & \mathbf{r}(1) = \mathbf{r}_f. \end{array}$$

The solution of this problem is written in the form of Picard iterations

$$\mathbf{v}^i(\tau) = \mathbf{v}(-1) + \int_{-1}^{\tau} \mathbf{g}\left(q, \mathbf{v}^{i-1}(q), \mathbf{r}^{i-1}(q)\right) dq,$$

$$\mathbf{r}^i(\tau) = \mathbf{r}(-1) + \int_{-1}^{\tau} \left(\mathbf{v}(-1) + \int_{-1}^{s} \mathbf{g}\left(q, \mathbf{v}^{i-1}(q), \mathbf{r}^{i-1}(q)\right) dq \right) ds,$$

with the notation $\dot{\mathbf{r}} = \mathbf{v}$ introduced. Further, the right sides of the equations [7] are approximated by the Chebyshev polynomials of the first kind

$$\mathbf{v}^i(\tau) = \sum_{k=0}^{P-1} \boldsymbol{\beta}_k^i T_k(\tau) = \mathbf{v}(-1) + \int_{-1}^{\tau} \sum_{k=0}^{P-2} \boldsymbol{F}_k^{i-1} T_k(q) dq,$$

$$\mathbf{r}^i(\tau) = \sum_{k=0}^{P} \boldsymbol{\alpha}_k^i T_k(\tau) = \mathbf{r}(-1) + \int_{-1}^{\tau} \sum_{k=0}^{P-1} \boldsymbol{\beta}_k^i T_k(s) ds,$$

where

$$\boldsymbol{F}_k^{i-1} = \sum_{j=0}^{M} V_{kj} W_{kj} \mathbf{g}\left(\tau_j, \mathbf{r}^{i-1}(\tau_j)\right) T_k(\tau_j);$$

$$W = \operatorname{diag}\left\{ \frac{1}{2}, 1, \ldots, 1, \frac{1}{2} \right\},$$

$$V = \operatorname{diag}\left\{ \frac{1}{M}, \frac{2}{M}, \ldots, \frac{2}{M}, \frac{1}{M} \right\},$$

when $M = P$, or

$$V = \operatorname{diag}\left\{ \frac{1}{M}, \frac{2}{M}, \ldots, \frac{2}{M}, \frac{2}{M} \right\},$$

when $M > P$. Here P is responsible for the order of approximation, and M corresponds to the number of points τ_j. The coefficients $\boldsymbol{\beta}_k^i$ are calculated by the formulas

$$\boldsymbol{\beta}_0^i = \boldsymbol{v}(-1) + \sum_{k=1}^{P-1} (-1)^{k+1} \boldsymbol{\beta}_k^i,$$

$$\boldsymbol{\beta}_1^i = \frac{1}{2}\left(2\boldsymbol{F}_0^{i-1} - \boldsymbol{F}_2^{i-1}\right),$$

$$\boldsymbol{\beta}_k^i = \frac{1}{2k}\left(\boldsymbol{F}_{k-1}^{i-1} - \boldsymbol{F}_{k+1}^{i-1},\right), \quad k = 2, 3, \ldots, P-3,$$

$$\boldsymbol{\beta}_{P-2}^i = \frac{\boldsymbol{F}_{P-3}^{i-1}}{2(P-2)},$$

$$\boldsymbol{\beta}_{P-1}^i = \frac{\boldsymbol{F}_{P-2}^{i-1}}{2(P-1)}.$$

For the coefficients $\boldsymbol{\alpha}_k^i$

$$\boldsymbol{\alpha}_0^i = \boldsymbol{x}(-1) + \sum_{k=1}^{P} (-1)^{k+1} \boldsymbol{\alpha}_k^i,$$

$$\boldsymbol{\alpha}_1^i = \frac{1}{2}\left(2\boldsymbol{\beta}_0^i - \boldsymbol{\beta}_2^i\right),$$

$$\boldsymbol{\alpha}_k^i = \frac{1}{2k}\left(\boldsymbol{\beta}_{k-1}^i - \boldsymbol{\beta}_{k+1}^i\right), \quad k = 2, 3, \ldots, N-2,$$

$$\boldsymbol{\alpha}_{P-1}^i = \frac{\boldsymbol{\beta}_{P-2}^i}{2(N-1)},$$

$$\boldsymbol{\alpha}_P^i = \frac{\boldsymbol{\beta}_{P-2}^i}{2P}.$$

The equations should be supplemented with the boundary conditions

$$\mathbf{v}(-1) = \sum_{k=0}^{P-1} \boldsymbol{\beta}_k^i T_k(-1),$$

$$\mathbf{v}(1) = \sum_{k=0}^{P-1} \boldsymbol{\beta}_k^i T_k(1),$$

$$\mathbf{r}(-1) = \sum_{k=0}^{P} \boldsymbol{\alpha}_k^i T_k(-1),$$

$$\mathbf{r}(1) = \sum_{k=0}^{P} \boldsymbol{\alpha}_k^i T_k(1).$$

As a stop criterion, it is possible to use

$$\left\|\mathbf{r}^{i+1}(t) - \mathbf{r}^i(t)\right\| < \varepsilon, \quad \left\|\mathbf{v}^{i+1}(t) - \mathbf{v}^i(t)\right\| < \varepsilon.$$

Appendix B

Algorithm 1 Multiple shooting technique based on the Chebyshev–Picard method.

$R, \Delta R, V, \Delta V, lr$
while *matching* is *false* **do**
  $V_{\text{new}}\ ,\ \Delta V_{\text{new}}\ \leftarrow updating\ (R)$
  $R_{\text{new}}\ ,\ \Delta R_{\text{new}}\ \leftarrow updating\,(R, V_{\text{new}}\ , lr)$
  if *check* is *true* **then**
    $R, \Delta R, V, \Delta V \leftarrow R_{\text{new}}\ , \Delta R_{\text{new}}\ , V_{\text{new}}\ , \Delta V_{\text{new}}$
  else
    $V_{\text{correct}}\ \leftarrow correction\,(V_{\text{new}}\ )$
    $R_{\text{new}}\ , \Delta R_{\text{new}}\ \leftarrow updating\,(R, V_{\text{correct}}\ , lr)$
    $V_{\text{new}}\ , \Delta V_{\text{new}}\ \leftarrow updating\,(R_{\text{new}}\ )$
    if *check* is *true* **then**
      $R, \Delta R, V, \Delta V \leftarrow R_{\text{new}}\ , \Delta R_{\text{new}}\ , V_{\text{new}}\ , \Delta V_{\text{new}}$
    else
      $R_{\text{correct}}\ \leftarrow correction\ (R)$
      $V_{\text{new}}\ , \Delta V_{\text{new}}\ \leftarrow updating\,(R_{\text{correct}}\ )$
      $R_{\text{new}}\ , \Delta R_{\text{new}}\ \leftarrow updating\,(R_{\text{correct}}\ , V_{\text{new}}\ , lr)$
      if *check* is *true* **then**
        $R, \Delta R, V, \Delta V \leftarrow R_{\text{new}}\ , \Delta R_{\text{new}}\ , V_{\text{new}}\ , \Delta V_{\text{new}}$
      else
        $R_{\text{average}}\ , V_{\text{average}}\ \leftarrow average(R, V)$
        $R_{\text{new}}\ , \Delta R_{\text{new}}\ \leftarrow updating\,(R_{\text{average}}\ , V_{\text{average}}\ , lr)$
        $V_{\text{new}}\ , \Delta V_{\text{new}}\ \leftarrow updating\,(R_{\text{new}}\ )$
        if *check* is *true* **then**
          $R, \Delta R, V, \Delta V \leftarrow R_{\text{new}}\ , \Delta R_{\text{new}}\ , V_{\text{new}}\ , \Delta V_{\text{new}}$
        else
          stop while
        end if
      end if
    end if
  end if
end while
return $R, \Delta R, V, \Delta V$

REFERENCES

[1] F. Topputo. On Optimal Two-Impulse Earth-Moon Transfers in a Four-Body Model. *Celestial Mechanics and Dynamical Astronomy*, 117:279–313, 2013.

[2] E. Belbruno and J. Miller. A Ballistic Lunar Capture Trajectory for the Japanese Spacecraft Hiten. Technical Report IOM 312/90.4-1731-EAB, JPL, California Institute of Technology, 1990.

[3] T. Hoffman. GRAIL: Gravity Mapping the Moon. In *Proceedings of the IEEE Aerospace Conference*, pages 293–300, Big Sky, Montana, USA, March 7-14, 2009.

[4] T. Gardner, B. Cheetham, A. Forsman, C. Meek, E. Kayser, J. Parker, M. Thompson, T. Latchu, R. Rogers, B. Bryant, and T. Svitek. CAPSTONE: A CubeSat Pathfinder for the Lunar Gateway Ecosystem. In *Proceedings of the 35th Annual Small Satellite Conference*, Logan, Utah, USA, August 7-12, 2021, 7 p.

[5] T. Gill. Lunar Orbital Platform-Gateway. In *45th Space Congress Proceedings*, Cape

Canaveral, Florida, USA, February 27 – March 1, 2018, 27 p.

[6] K. Oguri, K. Oshima, S. Campagnola, K. Kakihara, N. Ozaki, N. Baresi, Ya. Kawakatsu, and R. Funase. EQUULEUS Trajectory Design. *The Journal of the Astronautical Sciences*, 67:950–976, 2020.

[7] D. Folta, N. Bosanac, A. Cox, and K. Howell. The Lunar IceCube Mission Design: Construction of Feasible Transfer Trajectories with a Constrained Departure. *Advances in the Astronautical Sciences*, 158:1352–1369, 2016.

[8] D. McIntosh, J. Baker, and J. Matus. The NASA Cubesat Missions Flying on Artemis-1. In *Proceedings of the 34th Annual Small Satellite Conference*, Logan, Utah, USA, August 1-6, 2020, 11 p.

[9] J. Parker and R. Anderson. *Low-Energy Lunar Trajectory Design*. John Wiley & Sons, Pasadena, California, 2014.

[10] A. Tselousova, M. Shirobokov, and S. Trofimov. Geometrical Tools for the Systematic Design of Low-Energy Transfers in the Earth-Moon-Sun System. *Advances in the Astronautical Sciences*, 175:5233–5250, 2020.

[11] A. Tselousova, S. Trofimov, and M.Shirobokov. Geometric Approach to the Design of Lunar-Gravity-Assisted Low-energy Earth-Moon Transfers. In *Proceedings of the 2021 AAS/AIAA Astrodynamics Specialist Conference*, Big Sky, Montana, USA (Virtual), August 8-12, 2021, 20 p.

[12] R. Castelli. Regions of Prevalence in the Coupled Restricted Three-Body Problems Approximation. *Communications in Nonlinear Science and Numerical Simulation*, 17(2):804–816, 2012.

[13] W. Folkner, J. Williams, D. Boggs, R. Park, and P. Kuchynka. The planetary and lunar ephemerides de430 and de431. *IPN Progress Report*, 42-196, 2014, 81 p.

[14] C. Clenshaw and H. Norton. The Solution of Nonlinear Ordinary Differential Equations in Chebyshev Series. *The Computer Journal*, 6(1):88–92, 1963.

[15] J. Junkins, A. Younes, R. Woollands, and X. Bai. Picard Iteration, Chebyshev Polynomials and Chebyshev-Picard Methods: Application in Astrodynamics. *The Journal of the Astronautical Sciences*, 60:623–653, 2013.